Journal of Power Sources 196 (2011) 3942–3948

Contents lists available at ScienceDirect

Journal of Power Sources

journal homepage: www.elsevier.com/locate/jpowsour

Cycle-life model for graphite-$LiFePO_4$ cells

John Wang[a,*], Ping Liu[a], Jocelyn Hicks-Garner[a], Elena Sherman[a], Souren Soukiazian[a], Mark Verbrugge[b], Harshad Tataria[b], James Musser[c], Peter Finamore[c]

[a] HRL Laboratories, LLC, Malibu, CA 90265, United States
[b] General Motors Corp., Warren, MI 48092, United States
[c] John Deere Southeast Engineering Center, Charlotte, NC 28241, United States

ARTICLE INFO

Article history:
Received 25 October 2010
Received in revised form
22 November 2010
Accepted 23 November 2010
Available online 1 December 2010

Keywords:
$LiFePO_4$ battery
Life model
Cell aging
Cycle life

ABSTRACT

In this report, cycling induced capacity fade of a $LiFePO_4$ battery was studied and cycle-life models were established. Cell life data for establishing the model were collected using a large cycle-test matrix. The test matrix included three parameters, temperature (−30 to 60 °C), depth of discharge (DOD) (90–10%), and discharge rate (C-rate, ranging from C/2 to 10C, with the 1C rate corresponding to 2A). At the low C-rates, experimental results indicated that the capacity loss was strongly affected by time and temperature, while the DOD effect was less important. At the high C-rates, the charge/discharge rate effects became significant. To establish a life model, we adopt a power law equation in which the capacity loss followed a power law relation with time or charge throughput while an Arrhenius correlation accounted for the temperature effect. This model, when parameters were allowed to change with C-rates, was found to represent a large array of life cycle data. Finally, we discuss our attempts in establishing a generalized battery life model that accounts for Ah throughput (time), C-rate, and temperature.

1. Introduction

At present, lithium-ion batteries are increasingly being used to meet the energy and power demands of current consumer electronics. These batteries are also being targeted for use in the automotive and space industries. However, not knowing a battery's rate of capacity loss or useful life in these applications poses a significant business risk. For the automotive industry, this information is critical in determining the performance and durability of the battery in traction applications; for the space industry, the battery must last for the life of the mission as service and/or replacement is rarely an option.

Over the past few years there have been substantial efforts focused on the development of models to predict capacity fade in lithium ion batteries [1–12]. Different models have been developed to account for various scenarios responsible for capacity fade such as parasitic side reactions [5,13,14], SEI formation [6], and resistance increase [1,15,10]. However, experimental data are essential for the study of the aging processes of a battery system and the validation of the capacity fading mechanisms. To provide the required information, a significant amount of testing and a systematic modeling effort is needed to develop a reliable model to describe the factors effecting battery life. Very few groups have attempted to develop a life prediction model using a large experimental data set. Wright et al., [16–18] presented the testing results and life modeling of lithium-ion batteries with Ni based lithium insertion cathodes including $LiNi_{0.8}Co_{0.2}O_2$ and $LiNi_{0.8}Co_{0.15}Al_{0.05}O_2$. These results underscore the importance of using large testing matrix to investigate and validate the life modeling of lithium ion batteries.

$LiFePO_4$ (lithium iron phosphate) based lithium ion battery has been considered as one of most promising candidates for large scale applications in the automotive and space industries because of its excellent chemical and thermal stability and low cost [19–23]. However, capacity fade behavior and life modeling for this battery has not been well established. More importantly, there is little insight regarding the aging mechanisms associated with this type of battery [24–28]. We evaluated the aging mechanisms of $LiFePO_4$ lithium ion battery cells using both destructive physical analysis and non-destructive electrochemical analysis. The results indicate that capacity fade is primarily the result of loss of active lithium that is most likely associated with anode degradation [28].

This paper focuses on developing a semi-empirical life model based on this mechanism. The effects of four experimental parameters—time, temperature, depth of discharge (DOD), and discharge rate—were investigated. At low charge/discharge rates, the results suggest capacity loss is strongly affected by time and temperature, and the DOD effect is less important. A general power law equation described by Bloom et al. [29], where capacity fade follows a power law relation with time, was adopted as a starting point to develop our model. Initial results demonstrated that

* Corresponding author. Tel.: +1 310 317 5155; fax: +1 310 317 5840.
E-mail address: jswang@hrl.com (J. Wang).

0378-7753/$ – see front matter © 2010 Elsevier B.V. All rights reserved.
doi:10.1016/j.jpowsour.2010.11.134

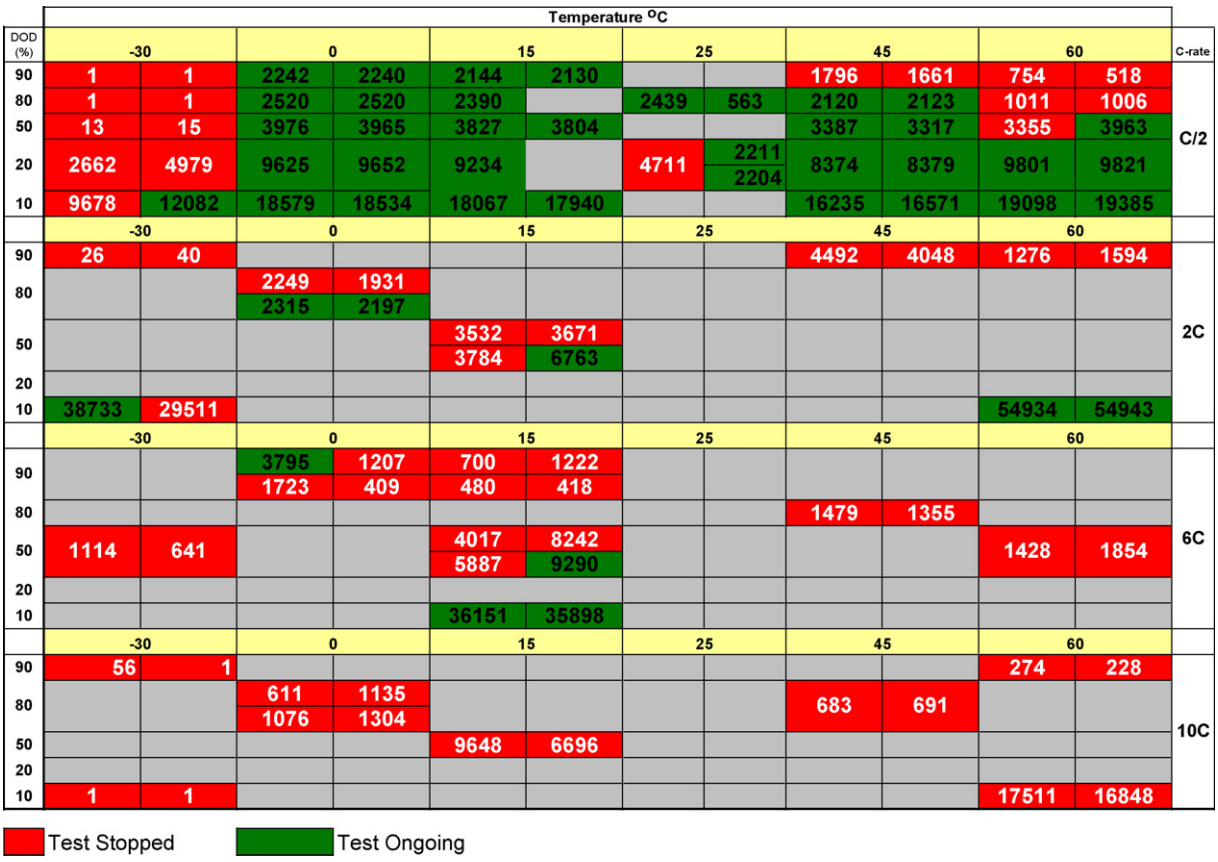

Fig. 1. Test matrix for accelerated cycle life study. Two cells were tested at each condition. The numbers in the test matrix indicate the number of cycles attained by the cell. Cells highlighted in green were still cycling when this manuscript was written, and cells highlighted in red have reached the defined end of life condition. (For interpretation of the references to color in this figure legend, the reader is referred to the web version of the article.)

the power law relationship can represent most of the life cycle data. Furthermore, the power law relation was used to establish a model to account for effect of C-rate over the range of C/2, 2C, 6C, and 10C.

2. Experimental

2.1. Test matrix

The commercially available 2.2 Ah, 26650 cylindrical cells were purchased from A123 Systems in which the material chemistry is composed of $LiFePO_4$ cathode and carbon anode. These lithium-ion cells were tested under the conditions given in the test matrix shown in Fig. 1. Two cells were tested at each of the conditions. These conditions include five different temperatures (−30, 0, 15, 25, 45, 60 °C), five levels of DOD (90%, 80%, 50%, 20% and 10%), and four discharges rates (C/2, 2C, 6C and 10C). In defining the DOD and C rates, the cell is de-rated to 2 Ah. Consequently, C rate corresponds to a current of 2 A. The cut-off voltages for the cycle test of all the cells were at 3.6 and 2.0 V. The constant current charge rates were C/2 for the C/2 discharge rate and 2C for higher discharge rates. The cells were charged to 3.6 V and held at 3.6 V until the current dropped below 0.1 A for a maximum of 2 days. The numbers in the matrix represent the cycle numbers that have been performed at each of those conditions. The cells highlighted in green are still being tested, and the cells highlighted in red indicate that they have reached End of Life (EOL) which is defined as failing to deliver the required capacity before reaching a cell voltage of 2.0 V.

2.2. Characterization

Prior to cycling tests, each cell was characterized using these four techniques: (1) capacity characterization, (2) relaxation test, (3) electrochemical impedance spectroscopy (EIS), and (4) hybrid pulse power characterization (HPPC). Detailed procedures of each technique are described in the following: (1) For capacity characterization, the cell was fully charged and then discharged at rates of 6C, C/2 and C/20. At each rate, two cycles were recorded and the capacity from the second cycle was used as the cell capacity. (2) For the relaxation test, a fully charged cell was discharged for a period of 24 min at C/2 rate, and then followed by a 2 h rest before the subsequent discharge. The test was complete when the discharge voltage reached 2 V. (3) The EIS characterization was performed at 40% state of the charge (SOC) which was defined as 72 min of discharge at C/2 rate of a fully charged cell. The EIS measurement was carried out in a frequency range between 0.01 and 100 kHz and AC amplitude of 5 mV. (4) For HPPC characterization, prior to a pulse power sequence, a fully charged cell was discharged to 10% DOD at 1C rate, and then rested for 1 h. The pulse power sequence was composed of three steps: (1) 5C discharge for 18 s, (2) rest at OCV for 32 s, and, (3) 3.75C charge for 10 s. After the pulse sequence, the cell was immediately discharged to 20% DOD and rested for 1 hr before the pulse power sequence was repeated. The cell was tested at 10% DOD increments until reaching the cut-off voltage of 2 V.

During life cycle test, cells were stopped periodically for characterization using the procedures described above. For example, at a low rate of C/2, the characterization procedures were performed for every 1 or 2 months between cycling test. At high rates, the time intervals for characterization were shorter.

For each of the cells tested, the cell capacity measured at a C/2 rate during characterization was used for the subsequent modeling work. The capacity loss was normalized with its initial cell capacity.

3. Results and discussion

The large test matrix, comprehending time, temperature, DOD and rate (Fig. 1), permits statistical evaluation of the factors effecting cycle life (capacity fade) and provide sufficient data for model development. Test conditions (2C through 10C) were chosen by performing a design of experiment (DOE) analysis [20], while all conditions were studied at C/2 discharge rates. In both cases, two cells were cycled at each condition to improve the robustness of the results. Many of the cells cycled at higher rates had reached the defined end of life condition (highlighted in red). Capacity fade at high discharge rates was accelerated as compared to C/2 discharge rates. Many cells cycled at the lower discharge rate were still cycling at the time of publication (highlighted in green). As shown in Fig. 1, cells at the extreme temperatures also performed poorly; i.e., they exhibited a high rate of capacity fade. The data indicate cells used at strenuous conditions, such as elevated temperatures and fast discharge rates, tend to have a shorter useful life.

Capacity characterization data were used to quantify the capacity fade rate for the model development. As an example, Fig. 2 shows the discharge curves obtained at a C/2 rate (after different number of cycles) for the cells cycled under the following conditions: A, 90% DOD, C/2, 0 °C; B, 90% DOD, C/2, 45 °C; and C, 90% DOD, C/2, 60 °C. As cells age upon cycling, the measured capacities decrease steadily, while the shape of discharge profiles remained unchanged. These cycle number dependent capacity loss data were collected for the cycle life model development. The functional form of the life model can be expressed as:

$$Q_{loss} = f(t, T, \text{DOD}, \text{Rate}) \quad (1)$$

where t is the cycling time, T is the test temperature, DOD is the depth-of-discharge, and Rate is the discharge rate for the cycle testing.

In the following sections, the effect of each parameter on cell life is investigated and described. In addition a model to describe the impact of these factors at low and high discharge rates is presented.

3.1. DOD and temperature effects

At a given C-rate, cells cycled at DODs greater than 50% were shown to reach the defined end of life condition sooner than those cycled at lower DODs (<50%). This observation is illustrated in Fig. 3, where capacity retention as a function of cycle number at various DODs for the cells at 60 °C and C/2 rate is plotted. When plotted in this manner capacity fade appears to be a function of DOD. However, when the same data is plotted as a function of time as shown in Fig. 4, the results indicate DOD has very little effect on capacity fade. The capacity fade rate was found to be approximately the same at each DOD indicating that the effect of cycling time is more significant than DOD. After a closer examination of all the DOD data at C/2 rate, we concluded that the DOD effect was not important for the conditions investigated. Thus, the DOD effect was not considered for formulating a model for at low discharge rates.

After eliminating DOD, capacity fade can only be affected by time (t) and temperature (T), at C/2 discharge rate (Eq. (1)). In this case, we adopt the following battery life model [29]:

$$Q_{loss} = B \cdot \exp\left(\frac{-E_a}{RT}\right) t^z \quad (2)$$

Instead of using time, we chose Ah-throughput as a parameter for the life modeling. Ah-throughput represents the amount of

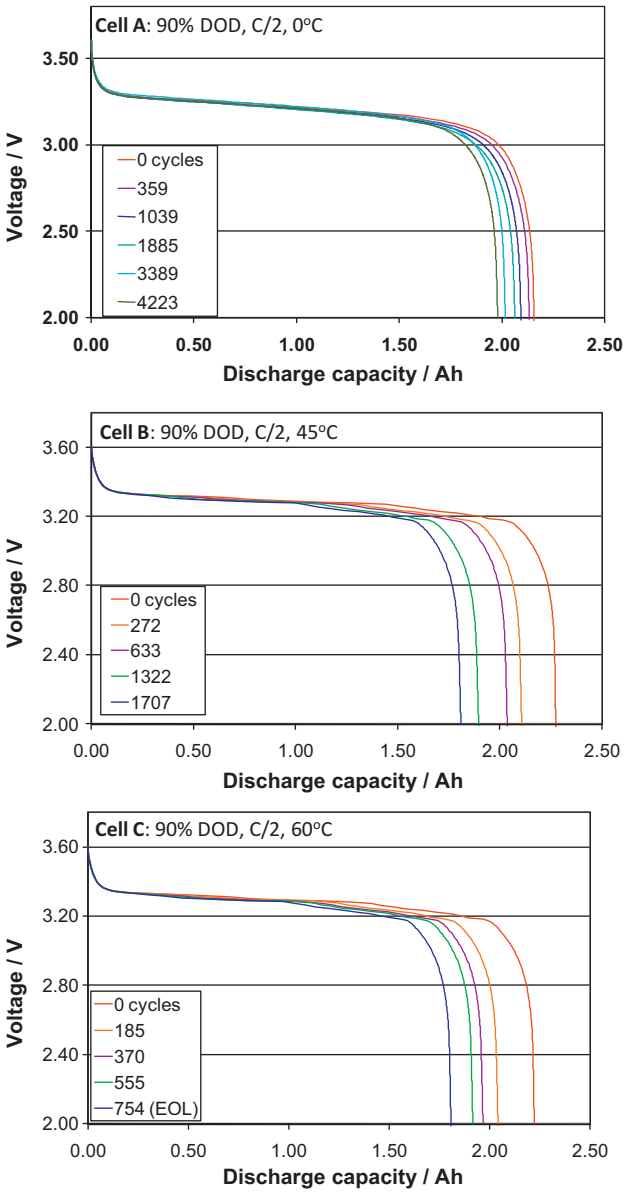

Fig. 2. Discharge curves of the battery cells cycled at three different conditions: (Cell A) 90% DOD, C/2, 0 °C; (Cell B) 90% DOD, C/2, 45 °C; and (Cell C) 90% DOD, C/2, 60 °C.

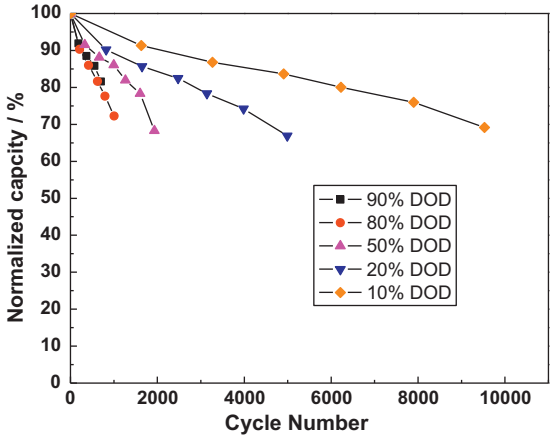

Fig. 3. Capacity retention at 60 °C and a discharge rate of C/2 plotted as a function of cycle number, data shown for 90(■), 80(●), 50(▲), 20(▼), and 10(◆)% DOD.

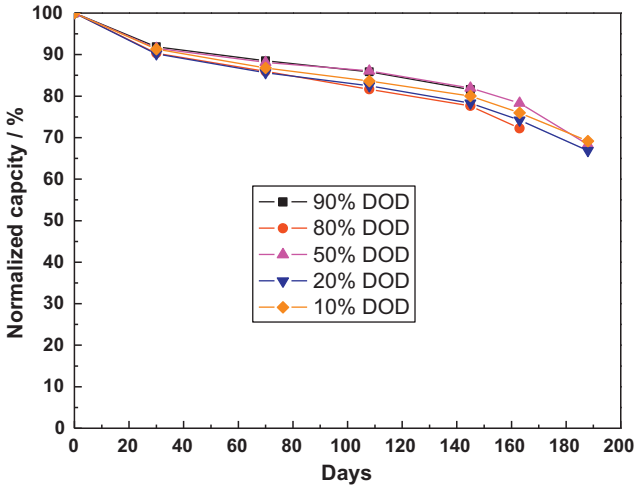

Fig. 4. Capacity retention at 60 °C and a dischare rate of C/2 plotted as a function of time (days), data shown for 90(■), 80(●), 50(▲), 20(▼), and 10(◆)% DOD.

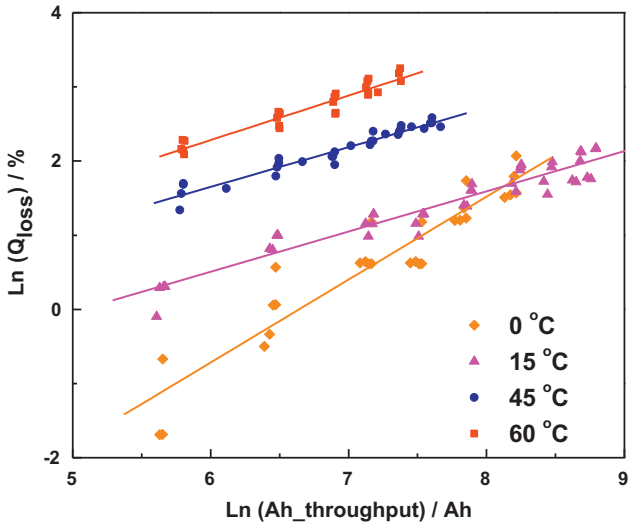

Fig. 5. Fit achieved when using equation to predict capacity loss as a function of temperature. Capacity loss is plotted as a function of Ah throughput at 0(◆), 15(▲), 45(●) and 60(■) °C. Substantial linearity is achieved at each temperature. (Data from each DOD and C/2 discharge rates are shown.)

charge delivered by the battery during cycling. At each C-rate, Ah-throughput is directly proportional to time; however, the merit of using Ah-throughput is that it allows us to quantify and correlate the capacity fading behaviors for different C-rates. The life model can be expressed as:

$$Q_{\text{loss}} = B \cdot \exp\left(\frac{-E_a}{RT}\right)(A_h)^z \quad (3)$$

In Eq. (3), Q_{loss}, is the percentage of capacity loss, B is the pre-exponential factor, E_a is the activation energy in J mol^{-1}, R is the gas constant, T is the absolute temperature, and A_h is the Ah-throughput, which is expressed as A_h = (cycle number) × (DOD) × (full cell capacity), and z is the power law factor.[1] Clearly, the exponent term represents that the temperature follows Arrhenius Law. For analytical purposes, we rearrange this slightly to

$$\ln(Q_{\text{loss}}) = \ln(B) - \left(\frac{E_a}{RT}\right) + z\ln(A_h) \quad (4)$$

In Fig. 5, the percentage of capacity loss is plotted as a function of Ah-throughput on a logarithmic scale at 0, 15, 45 and 60 °C. The lines represent the linear fit at each temperature. −30 °C data were not plotted because the cells at this temperature generally do not cycle long enough to produce sufficient data (we note that given the manufacturer specifications the cells were not expected to perform at some of the conditions, e.g. 90% DOD). According to Eq. (4), the slope of the each line at each of the temperatures evaluated represents the power law factor, z. As shown in Fig. 5, the fitted lines are parallel to each other at 15, 45 and 60 °C, indicating that the slopes of these lines are very similar. These results suggest that the temperature effect is independent of the power law factor z. At 0 °C, the steep slope suggests that other mechanisms maybe responsible for the observed accelerated capacity loss. AC impedance data (not shown) also revealed that the charge transfer resistance was significantly higher at 0 °C than at room temperature, which could introduce other decay mechanisms. Consequently, the 0 °C data was excluded at this stage of the empirical fitting.

3.2. Life model development for C/2 rate

To determine the fitting parameters, we implemented a single step optimization process using Equation 4 with a slight rearrangement of the terms. The graphical representation of this method is shown in Fig. 6 where $\ln(Q_{\text{loss}}) + E_a/RT$ is plotted as a function of $\ln(A_h)$. The activation energy E_a was obtained from the intercept values of the best-fit nonlinear regression curves. Applying the experimental data from 15, 45 and 60 °C at C/2 discharge rates, E_a was found to be close to 31,500 J mol^{-1}. Judging from the fitted linear relations, the effect of temperature indeed follows an Arrhenius relation, which often corresponds to a thermally activated chemical process, such as a chemical side reaction that occurs during cycling, potentially SEI layer formation [6,30]. The pre-exponential factor B can be determined from the intercept of the linear fittings shown in Fig. 6. The slope of line represents the power law factor z, which is equal to 0.552. Interestingly, this value is very close to 0.5 which represents a square-root of time dependence. Previous reports [6,17,30] have indicated that this square-root of time relationship with capacity fade represents the irreversible capacity loss due to solid electrolyte interface (SEI) growth that consumes active lithium and is often controlled by a diffusion process.

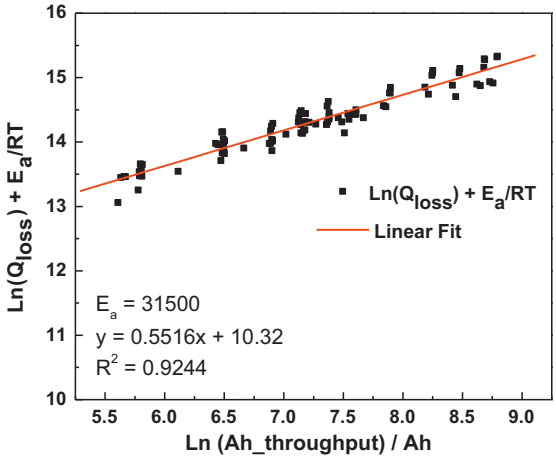

Fig. 6. Use of Eq. (4) to determine the fitting parameters for the life prediction model in which $\ln(Q_{\text{loss}}) + E_a/RT$ is plotted as a function of ln(time). (Data from all levels of DOD at C/2 rate are included.) The activation energy E_a was obtained from the best-fit values determined by nonlinear regression, R^2. The slope and intercept of the linear fitting correspond to the power law factor, z, and the pre-exponent value, A, respectively.

[1] Cells were de-rated to 2Ah for the full cell capacity.

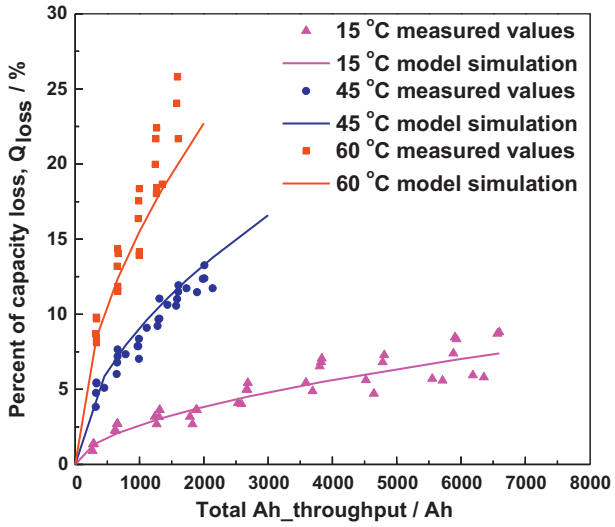

Fig. 7. Simulation of cycle-life prediction model (line) and experimental data (dots) at 15(▲), 45(◆), 60(■) °C and a C/2 discharge rate. (Data from each experimental DOD is included).

Table 1
Equation to predict capacity fade at a given discharge rate.

C-rates	Life model
C/2	$Q_{loss} = 30,330 \cdot \exp(-31,500/RT) \cdot (A_h)^{0.552}$
2C	$Q_{loss} = 19,300 \cdot \exp(-31,000/RT) \cdot (A_h)^{0.554}$
6C	$Q_{loss} = 12,000 \cdot \exp(-29,500/RT) \cdot (A_h)^{0.56}$
10C	$Q_{loss} = 11,500 \cdot \exp(-28,000/RT) \cdot (A_h)^{0.56}$

As a result, the capacity loss life model is expressed as:

$$Q_{loss} = 30,330 \exp\left(\frac{-31,500}{8.314T}\right) A_h^{0.552} \quad (5)$$

Using the life model in Eq. (5), we are able to simulate qualitatively the capacity fade under various conditions. In Fig. 7, simulations of the capacity fade at different temperatures are compared to experimental data. Overall, the life model appears to be in a general agreement with the experimental data. The model slightly underestimates capacity loss at 60 °C and overestimates capacity loss at 45 °C. Our results demonstrate that at the low rates, time and temperature are the two parameters that substantially affect capacity fade and that DOD has a negligible effect on capacity fade.

3.3. Life modeling for high C-rates

We further examined whether this function form of the life model could predict capacity fade behavior at high discharge rates (>C/2). First, we proceeded to use Eq. (4) to fit the capacity fade profile at each discharge rate (2C, 6C and 10C). We found that the experimental data do follow the power law relation. At a 2C discharge rate the E_a and z values obtained (Table 1) are comparable to those values for C/2 rate suggesting that the factors effecting capacity fade are similar at low and high discharge rates. Therefore, we used this power law relation as a basis to fit the capacity loss at 6C and 10C discharge rates as well. For 6C and 10C rates, because there are fewer data points collected (from the capacity characterization data) prior to the cell reaching the defined EOL condition, curve fitting techniques were used to numerically fit the experimental data with the power law equation (Eq. (3)) at each of the cycling conditions. Specifically, using Eq. (3), we fit each of the cycle conditions simultaneously to obtain the values of B, E_a, and z. For each constant C-rate, we find the optimal parameter values of B, E_a, and z, by minimizing the total error. This total error is defined as:

$$\varepsilon_{opt} = \sum_{j=N} [Q_{loss,j}^{measured} - Q_{loss,j}^{model}]^2 \quad (6)$$

where j represents each of the cycled conditions. The optimal values were found for each rate using Newton's iteration method with the aid of the SOLVER function in EXCEL. The results are summarized in Table 1.

Table 2
Average actual cell temperatures, measured during cycling, conditions indicated below.

% DOD	0 °C	15 °C	25 °C	45 °C	60 °C	
90	7.76	–	26.40	–	–	2C
80	7.59	–	26.41	–	–	
50	6.92	–	26.33	–	–	
10	4.54	–	26.06	–	–	
90	13.90	18.60	27.82	47.24	–	6C
80	13.95	18.42	27.71	47.18	–	
50	13.34	17.95	27.51	46.99	–	
10	9.03	16.98	27.00	46.69	–	
90	17.90	19.32	28.71	48.16	63.20	10C
80	17.99	19.22	28.59	48.02	63.04	
50	17.47	19.01	28.29	47.78	62.74	
10	11.62	17.94	27.58	47.30	62.60	

We note that actual cell temperatures (instead of environmental temperatures) were used for numerical fitting of the life model equation at the high discharge rates. Cell heating during cycling becomes more significant when the cell is discharged at a high rate. Table 2 shows the average temperatures measured at the surface of the battery cell during cycling. Particularly at low environmental temperatures, the real cell temperatures increase considerably during the discharge. In addition, the cells cycled at higher DODs tend to heat up more than those cycled at lower DODs.

While the above analysis indicates that we are able to establish a life model using the power law relation at each C-rate (Table 1), it is of great interest to develop a generalized equation to describe the capacity fade behavior for all conditions. A closer examination on the magnitudes of activation energy E_a values revealed that we could be fit the data if E_a decreased with increasing C-rate. This trend allowed us to establish a mathematical correlation to account for the rate effects. The power law factor z, on the other hand, remained fairly constant at all C-rates. Therefore, we set the z value at 0.55 for all conditions. The function form of the life model can be expressed as:

$$Q_{loss} = B \cdot \exp\left[\frac{-31700 + 370.3 \times \text{C\_Rate}}{RT}\right] (A_h)^{0.55} \quad (7)$$

It appears that there is a general trend for the pre-exponent factor B, in which the value decreases with increasing C-rate. However, it is difficult to quantitatively describe this relationship by using a simple mathematical correlation. Instead, using Eq. (7), we simultaneously fitted the experimental data for all C-rates. The optimal values of B were found for each C-rate by minimizing the total error using Eq. (6). The results are summarized in Table 3. Using this unified life model equation, we are able to describe qualitatively the capacity fading behaviors for all conditions. In Fig. 8, simulation results obtained with the life model equation are compared with

Table 3
Generalized life model for all C-rates.

$Q_{loss} = B \cdot \exp[(-31,700 + 370.3 \times \text{C\_Rate}/RT](A_h)^{0.55}$
$A_h = \text{cycle\_number} \times \text{DOD} \times 2$

C-rate	C/2	2C	6C	10C
A values	31,630	21,681	12,934	15,512

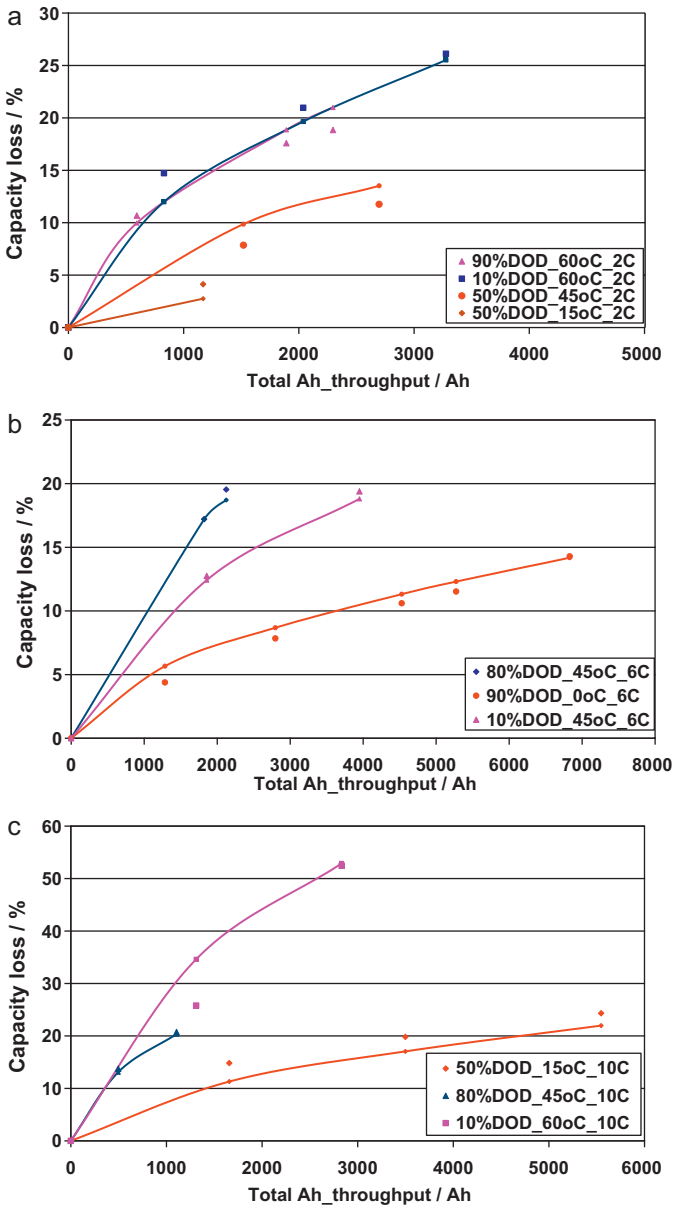

Fig. 8. Model simulation results (lines) and experimental results (dots) at 2C (a), 6C (b) and 10C (C) discharge rates.

the measured capacity loss data for 2C, 6C and 10C rates. The model projections are consistent with the experimental data for all the C-rates.

A closer examination of the established model reveals additional insight relative to aging mechanisms responsible for the capacity fade. For example, the power law factor, z is very close to 0.5, leading to a square-root of time relationship. Previous reports have indicated that the rate of lithium consumption at the negative carbon electrode due to SEI formation has a square root of time dependence [6,17,30]. In addition, our prior findings using destructive physical analysis and non-destructive electrochemical analysis established that the capacity fade is caused by the loss of active lithium most likely associated with the carbon anode degradation [28]. Consequently, our modeling results are consistent with the aging mechanism that the active lithium is consumed to repair and/or grow the SEI layer when the carbon anode is cracked due to anode degradation. In addition, there is also a C-rate effect. The Arrhenius law used in the model equation represents the kinetics of the chemical processes for the undesired side reactions such as for SEI formation. The inverse relationship of the magnitude of activation energy with the C-rate suggests that higher rates produce higher diffusion induced stress field [31] on the particles which accelerates the chemical processes that cause irreversible active lithium consumption.

We have demonstrated that this rather simple life model represents qualitatively the experimental data for all the rates investigated. It is also recognized that the accuracy of the life model predictions at the high rates produce slightly more error than at the low rates. Overall, this generalized approach allows us to present quantitative projections of capacity fading behaviors for a wide range of cycling conditions.

4. Conclusion

In this report, we have presented the cycling test results from an accelerated cycle life study on commercially available $LiFePO_4$ batteries. The effects of test parameters (time, temperature, DOD, rate) were investigated and described. The results show that the capacity loss is strongly affected by time and temperature, while the effect of DOD is less important at a C/2 discharge rate. A life model was developed to describe the time and temperature dependence of capacity fade at this low discharge rate. Using a curve-fitting technique, we demonstrated that capacity fade followed a power law relationship with charge throughput between 15 °C and 60 °C. The established power law model was used as a basis to develop a model equation to describe capacity fade at each higher discharge rate (2C, 6C and 10C). For all C-rates, the model equations indicated that power law factors were valued very close to 0.5. This square-root of time dependence is consistent with the aging mechanisms that involve diffusion and parasitic reactions leading to loss of active lithium. Overall, we were able to establish a simple battery life model that accounts for Ah throughput (time), C-rates, and temperature and achieves qualitative agreement with experimental data. We note in closing that the model should be applicable to other lithium ion batteries as long as the aging mechanisms are similar. In contrast, we excluded data from 0 °C in the present study in formulating the current model. Experimental observations indicate a change in the decay mechanism might be operative at lower temperatures, and this remains an open question.

References

[1] T.F. Fuller, M. Doyle, J. Newman, J. Electrochem. Soc. 141 (1994) 1.
[2] C. Fellner, J. Newman, J. Power Sources 85 (2000) 229.
[3] J. Christensen, J. Newman, J. Solid State Electrochem. 10 (2006) 293.
[4] B.Y. Liaw, R.G. Jungst, G. Nagasubramanian, H.L. Case, D.H. Doughty, J. Power Sources 140 (2005) 157.
[5] P. Ramadass, B. Haran, P.M. Gomadam, R. White, B.N. Popov, J. Electrochem. Soc. 151 (2004) A196.
[6] R. Spotnitz, J. Power Sources 113 (2003) 72.
[7] B. Wu, M. Mohammed, D. Brigham, R. Elder, R.E. White, J. Power Sources 101 (2001) 149.
[8] P.M. Gomadam, J.W. Weidner, R.A. Dougal, R.E. White, J. Power Sources (2002) 267.
[9] S. Santhanagopalan, Q.Z. Guo, P. Ramadass, R.E. White, J. Power Sources 156 (2006) 620.
[10] M. Dubarry, B.Y. Liaw, J. Power Sources 174 (2007) 856.
[11] M. Safari, M. Morcrette, A. Teyssot, C. Delacourt, J. Electrochem. Soc. 156 (2009) A145.
[12] G. Ning, B.N. Popov, J. Electrochem. Soc. 151 (2004) A1584.
[13] R. Darling, J. Newman, J. Electrochem. Soc. 145 (1998) 990.
[14] G. Ning, R.E. White, B.N. Popov, Electrochim. Acta 51 (2006) 2012.
[15] J. Christensen, J. Newman, J. Electrochem. Soc. 150 (2003) A1416.
[16] R.B. Wright, J.P. Christophersen, C.G. Motloch, J.R. Belt, C.D. Ho, V.S. Battaglia, J.A. Barnes, T.Q. Duong, R.A. Sutula, J. Power Sources 119 (2003) 865.
[17] R.B. Wright, C.G. Motloch, J.R. Belt, J.P. Christophersen, C.D. Ho, R.A. Richardson, I. Bloom, S.A. Jones, V.S. Battaglia, G.L. Henriksen, T. Unkelhaeuser, D. Ingersoll, H.L. Case, S.A. Rogers, R.A. Sutula, J. Power Sources 110 (2002) 445.
[18] I. Bloom, S.A. Jones, E.G. Polzin, V.S. Battaglia, G.L. Henriksen, C.G. Motloch, R.B. Wright, R.G. Jungst, H.L. Case, D.H. Doughty, J. Power Sources 111 (2002) 152.

[19] A.K. Padhi, K.S. Nanjundaswamy, J.B. Goodenough, J. Electrochem. Soc. 144 (1997) 1188.
[20] N. Ravet, Y. Chouinard, J.F. Magnan, S. Besner, M. Gauthier, M. Armand, J. Power Sources 97/98 (2001) 503.
[21] N. Recham, L. Dupont, M. Courty, K. Djellab, D. Larcher, M. Armand, J.M. Tarascon, Chem. Mater. 21 (2009) 1096.
[22] B. Kang, G. Ceder, Nature 458 (2009) 190.
[23] S.Y. Chung, J.T. Bloking, Y.M. Chiang, Nat. Mater. 1 (2002) 123.
[24] M. Dubarry, B.Y. Liaw, J. Power Sources 194 (2009) 541.
[25] K. Striebel, A. Guerfi, J. Shim, M. Armand, M. Gauthier, K. Zaghib, J. Power Sources 119 (2003) 951.
[26] J. Shim, K.A. Striebel, J. Power Sources 119 (2003) 955.
[27] K. Striebel, J. Shim, A. Sierra, H. Yang, X.Y. Song, R. Kostecki, K. McCarthy, J. Power Sources 146 (2005) 33.
[28] P. Liu, J. Wang, J. Hicks-Garner, E. Sherman, S. Soukiazian, M.W. Verbrugge, H. Tataria, J. Musser, P. Finamore, J. Electrochem. Soc. 157 (2010) A499.
[29] I. Bloom, B.W. Cole, J.J. Sohn, S.A. Jones, E.G. Polzin, V.S. Battaglia, G.L. Henriksen, C. Motloch, R. Richardson, T. Unkelhaeuser, D. Ingersoll, H.L. Case, J. Power Sources 101 (2001) 238.
[30] M. Broussely, S. Herreyre, P. Biensan, P. Kasztejna, K. Nechev, R.J. Staniewicz, J. Power Sources 97/98 (2001) 13.
[31] Y.T. Cheng, M.W. Verbrugge, J. Appl. Phys. 104 (2008) 6.